https://doi.org/10.5194/egusphere-2026-662
Preprint. Discussion started: 12 February 2026

Brief Communication: Retrieval-Driven Spread in Antarctic Winter Freeboards (CryoSat-2, 2013–2018)

Xinlong Liu[1,2], Stuart Paul Corney[1,2], Rachel Louise Tilling[3,4], and Petra Heil[5,2,6]

[1]Institute for Marine and Antarctic Studies, University of Tasmania, Battery Point, TAS, Australia
[2]Australian Antarctic Program Partnership, University of Tasmania, Battery Point, TAS, Australia
[3]Cryospheric Sciences Laboratory, NASA Goddard Space Flight Center, Greenbelt, MD, USA
[4]Earth System Science Interdisciplinary Center, University of Maryland, College Park, MD, USA
[5]Australian Antarctic Division, Kingston, TAS, Australia
[6]Institute for Snow and Avalanche Research, Swiss Federal Institute for Forest, Snow and Landscape Research, Davos, Switzerland

Correspondence: Xinlong Liu (xinlong.liu@utas.edu.au)

Abstract.

The accuracy of remotely-sensed Antarctic sea-ice thickness is limited by assumptions of snow properties and processing choices that are often informed from the Arctic. To quantify retrieval-driven spread, we compare winter radar freeboard and snow-corrected sea-ice freeboard from four CryoSat-2–era products for 2013–2018. All products reproduce the large-scale spatial structure, yet each shows systematic offsets relative to CCI that persist across multiple spatial scales. Both the Western Weddell and Ross Sea sectors display interannual variability, while correlation, bias and RMSE exhibit sector- and variable-dependent performance relevant to thickness.

1 Introduction

Antarctic sea-ice thickness is a key climate variable, modulating ocean–atmosphere exchange (Maykut, 1978; Kurtz et al., 2011) and integrating thermodynamic and dynamic forcing. Despite its importance its variability and trends remain difficult to constrain from space. A central contributor to this uncertainty is the deep, heterogeneous Antarctic snow cover, which alters Ku-band radar wave interaction with the snow–ice system and introduces large altimeter retrieval sensitivity relative to the Arctic (Willatt et al., 2009; Garnier et al., 2021), where many algorithms and snow parameterisations were originally developed.

Radar altimetry measures radar freeboard (h_{fr}), but thickness-relevant sea-ice freeboard (h_{fi}) requires a snow-propagation correction and other processing choices (Tilling et al., 2018; Mallett et al., 2020). For Antarctic sea ice, uncertainty in snow properties and the effective scattering horizon can therefore generate systematic, spatially coherent inter-product offsets (Kwok, 2014; Kacimi and Kwok, 2020) that propagate directly into thickness. Here, we quantify where four CryoSat-2–era products agree and diverge, from basin-scale winter means to sector-scale variability.

To provide a practical benchmark for CryoSat-2–era Antarctic winter freeboards, we intercompare four widely used radar-altimetry products (LEGOS, CCI, CSAO, and Cryo-TEMPO) over the period 2013–2018 (May-October) on a common 50 km

https://doi.org/10.5194/egusphere-2026-662
Preprint. Discussion started: 12 February 2026

grid (Garnier et al., 2019; Gaudelli et al., 2022; Paul et al., 2024; Andersen et al., 2025). Using CCI as a consistent reference frame for relative offsets, we quantify (1) the basin-scale magnitude and spatial coherence of inter-product differences in h_{fr} and h_{fi} and (2) agreement in interannual variability in two contrasting regimes (Western Weddell and Ross). Results are summarised with winter-mean maps and difference patterns (Figure 1), sector-mean time series (Figure 2), and compact performance statistics (correlation, bias, RMSE; Figure 3). By isolating retrieval-driven spread within a single-sensor era, we provide guidance on where improved Antarctic snow constraints and harmonised processing would have the largest impact on h_{fi} consistency.

2 Data and Methods

2.1 CryoSat-2 Freeboard Products (2013–2018)

We intercompare four publicly available Antarctic winter freeboard products derived from CryoSat-2/SIRAL Ku-band radar altimetry: ESA Sea Ice Climate Change Initiative (hereafter CCI; Paul et al., 2024; Rinne and Hendricks, 2024), LEGOS/C-TOH (LEGOS II; Garnier et al. (2019)), CryoSat+ Antarctic Ocean (CSAO; Gaudelli et al. (2022)), and CryoSat-2 ThEMatic Products (Cryo-TEMPO; Andersen et al. (2025)). The products share a common measurement principle but differ in key processing choices (e.g., retracking, sea-surface height anomaly retrieval, and snow-related assumptions embedded in the conversion from radar to sea-ice freeboard). To maintain a concise and reproducible intercomparison, we analyse the freeboard fields as distributed by each provider (i.e., without harmonising snow inputs).

We analyse two freeboard variables provided by each product: radar freeboard (h_{fr}), defined as the retracked Ku-band elevation relative to the local sea surface, and the corresponding sea-ice freeboard (h_{fi}) after each product's snow-related propagation correction and associated processing choices. For consistency of terminology, we denote the snow-related correction term as h_{sc}, such that $h_{fi} = h_{fr} + h_{sc}$ (equivalently, $h_{sc} = h_{fi} - h_{fr}$).

2.2 Common Winter Period, Grid, and Masking

We restrict the analysis to the austral winter season (defined here as May–October) and the common CryoSat-2 era 2013–2018, consistent with the availability and winter-focused design of several products and with established best practice for Antarctic Ku-band retrievals under cold, predominantly dry-snow conditions (e.g., Kacimi and Kwok (2020); Fons et al. (2023)). All products are analysed on the common 50 km × 50 km EASE-2 Southern Hemisphere grid. LEGOS II, CSAO, and Cryo-TEMPO fields are regridded onto the CCI grid using bilinear interpolation for continuous variables; grid cells flagged as fill/invalid in the source products remain masked after reprojection.

To ensure that product differences reflect retrieval choices rather than sampling/coverage, we apply a *common-mask* strategy. For each month, we retain only those grid cells where *all* products provide valid estimates for the variable under comparison; all other cells are excluded (shown as transparent in maps). Genuine zero values are retained as valid data. This common-mask is used for basin-scale difference maps (Figure 1) and for all sector-mean time series and summary metrics (Figs. 2–3).

https://doi.org/10.5194/egusphere-2026-662
Preprint. Discussion started: 12 February 2026

Basin-scale fields shown in Figure 1 are multi-year winter means computed by (i) averaging monthly fields over May–October for each year and (ii) averaging those winter means over 2013–2018. Difference maps are reported as relative offsets from CCI (product minus CCI), treating CCI as a practical reference on the shared grid rather than an absolute truth.

2.3 Sector Analysis and Intercomparison Metrics

To characterise regional structure we partition the circumpolar Antarctic sea-ice zone (90° S–50° S) into six standard longitude sectors (following Comiso and Nishio (2008)). Here we focus on two contrasting regions; the Western Weddell and Ross seas, with a full-sector analysis in the Supplement). For each sector and month, we compute sector-mean h_{fr} and h_{fi} as the arithmetic mean across common-mask grid cells (equal-area EASE-2 cells), yielding a monthly sector-mean time series for May–October 2013–2018. Interannual winter means (Figure 2) are then computed by averaging yearly May–October sector means.

We quantify inter-product agreement relative to CCI using (i) Pearson correlation coefficient r, (ii) mean bias (product minus CCI), and (iii) RMSE of the difference. Unless otherwise stated, these statistics are computed from the interannual winter-mean time series (2013–2018; Figure 3), ensuring consistent weighting of each winter and avoiding dominance by months with denser sampling.

3 Results

Here we present results for Antarctic-wide mean freeboards, followed by interannual variability for two key sectors: the Western Weddell and Ross Seas. These demonstrate (i) the basin-scale mean patterns and retrieval-driven differences in radar and derived sea ice freeboard (Figure 1), (ii) how those differences manifest in two contrasting sectors through time (Figure 2), and (iii) summarise agreement and offsets concisely with correlation, bias, and RMSE (Figure 3). Results for additional sectors and time periods are provided in the Supplement.

3.1 Basin-Scale Winter-Mean Structure and Coherent Difference Patterns

Across products, the multi-year winter-mean spatial structure is consistent for both radar and sea ice freeboards (Figure 1): higher freeboards occur in the Weddell and Ross seas and lower values occur in the Indian and Amundsen-Bellingshausen sectors. Consequently, product differences relative to CCI exhibit coherent, geographically structured patterns rather than spatially uncorrelated noise, indicating systematic sensitivity to retrieval choices.

Basin-scale offsets relative to CCI are systematic and sector-dependent (Figure 1; Table 1). For 2013–2018, LEGOS II retrieves higher radar freeboard than CCI in all six sectors, with $\Delta h_{fr} = \mathrm{LEGOS} - \mathrm{CCI}$ ranging from < 0.01 m (Pacific) to 0.06 m (Western Weddell) and typical positive offsets of 0.01–0.03 m elsewhere (Table 1). In contrast, CSAO and Cryo-TEMPO are lower than CCI for h_{fr} across all sectors, with Δh_{fr} of -0.01 to -0.04 m (CSAO) and -0.01 to -0.04 m (Cryo-TEMPO), reaching -0.04 m in the Western Weddell and Pacific sectors (Table 1).

https://doi.org/10.5194/egusphere-2026-662
Preprint. Discussion started: 12 February 2026

Differences are larger for sea-ice freeboard than for radar freeboard in several sectors (Figure 1; Table 1). For h_{fi}, LEGOS II remains higher than CCI in most sectors (typically 0.01–0.03 m), with a maximum positive bias of 0.05 m in Western Weddell, whereas CSAO is systematically lower by -0.03 to -0.07 m (largest in Western Weddell) and Cryo-TEMPO by -0.02 to -0.04 m (Table 1).

3.2 Interannual Variability: Shared Variability, Persistent Offsets, and the Role of h_{sc}

For the Western Weddell (high-snow, high-freeboard regime) and the Ross Sea (lower mean freeboard and a predominantly seasonal pack-ice regime; Figure. 2), interannual variability is broadly consistent among products, while absolute offsets persist.

The Western Weddell sector shows the largest separation relative to CCI in the CryoSat-2 era (2013–2018 winter means). LEGOS II is higher than CCI by 0.06 m in h_{fr} and 0.05 m in h_{fi}, whereas CSAO and Cryo-TEMPO are lower by $\sim$ 0.04 m in h_{fr} and by 0.07 m and 0.04 m in h_{fi}, respectively (product$-$CCI; Table 1). This yields an inter-product spread of $\sim$ 0.12 m in winter-mean h_{fi} in Western Weddell, and the separation increases from h_{fr} to h_{fi} where the snow-related correction is larger (h_{sc} ≈0.04–0.07 m; Table 1). The Ross sector exhibits the same qualitative ordering but with reduced offsets: LEGOS II is +0.02 m in both h_{fr} and h_{fi}, while CSAO and Cryo-TEMPO are lower by 0.01–0.02 m (h_{fr}) and 0.02–0.03 m (h_{fi}), giving a total h_{fi} spread of ∼0.05 m. The winter-mean h_{fi} spread is largest in the Western Weddell. This sector is widely documented as a high-snow regime with spatially distinct sea-ice topography/deformation, while the Ross sector generally has shallower snow depths; these contrasts provide a physical basis for enhanced retrieval sensitivity in the Western Weddell (Huang and Hajnsek, 2024; Willatt et al., 2025; Fredensborg Hansen et al., 2025).

The inclusion of h_{sc} (Figure 2) clarifies how snow-related assumptions contribute to h_{fi} divergence. Because $h_{fi} = h_{fr} + h_{sc}$, a product can show agreement in h_{fr} yet still diverge in h_{fi} if it applies systematically smaller (or larger) snow propagation corrections. This mechanism is most evident for CSAO: its h_{fr} can sit near CCI while its h_{fi} is lower, consistent with a smaller effective h_{sc} in these sectors. By contrast, LEGOS and Cryo-TEMPO offsets in h_{fi} largely follow their offsets in h_{fr}, implying that baseline radar-freeboard differences dominate their sea-ice freeboard separation, with h_{sc} differences playing a secondary role at sector-mean scale.

3.3 Summary Metrics Relative to CCI: High Correlations Do not Imply Agreement in Absolute Freeboard

Figure 3 intercompares correlation (r), bias, and RMSE relative to CCI for the Western Weddell and Ross sea sectors. Correlations indicate broadly consistent interannual variability: for h_{fr}, r =0.95 (LEGOS II) and 0.85 (Cryo-TEMPO) in Western Weddell and r =0.94 (LEGOS II) and 0.89 (Cryo-TEMPO) in Ross; for h_{fi}, r =0.79 for LEGOS II in Western Weddell and r =0.80 for CSAO in Ross, respectively. However, absolute offsets remain substantial and sector-dependent (Figure 3). In Western Weddell, LEGOS is biased high relative to CCI by $\sim+6$ cm in h_{fr} and +5–6 cm in h_{fi}, whereas Cryo-TEMPO is biased low by ~-4 cm (h_{fr}) and ~-5 cm (h_{fi}). CSAO has near-zero to ∼+1 cm bias in h_{fr} but a more negative bias in h_{fi} (~-1 to -2 cm), consistent with differences in the applied snow correction. Bias magnitudes are smaller in the Ross sector than in Western Weddell, reinforcing the interpretation that high-snow regimes amplify retrieval-driven divergence. Thus, even

https://doi.org/10.5194/egusphere-2026-662
Preprint. Discussion started: 12 February 2026

when r is high, centimetre-scale biases persist, indicating that agreement in variability does not imply agreement in absolute freeboard.

4 Discussion

This comparison is designed to clarify how retrieval choices, and in particular the snow-related conversion from h_{fr} to h_{fi}, shape product-to-product differences in CryoSat-2 era Antarctic winter freeboards (Figures. 1–3).

Because sea-ice freeboard is obtained by applying a snow-related correction to radar freeboard ($h_{fi} = h_{fr} + h_{sc}$), agreement in h_{fr} does not guarantee agreement in h_{fi}. Products can align in baseline h_{fr} yet diverge in h_{fi} if their effective snow propagation-speed correction (h_{sc}) differs in magnitude or spatial structure. Therefore, users should treat h_{sc} as a first-order source of inter-product spread and avoid interpreting close agreement in h_{fr} as evidence that h_{fi} (and derived thickness) will be consistent in absolute magnitude across products (i.e., have comparable baselines and small systematic offsets).

The Western Weddell sector provides a clear example of how larger snow-related corrections can amplify divergence in h_{fi} (Figure. 2). Where h_{sc} is larger, h_{fi} becomes more sensitive to assumptions about snow properties and the effective scattering horizon embedded in each retrieval. The CSAO behaviour illustrates the mechanism: it can be close to CCI in h_{fr} while remaining lower in h_{fi}, consistent with a smaller effective h_{sc} (Figures. 2–3). Practically, this implies that apparent agreement in h_{fr} can still yield materially different h_{fi} in the Western Weddell, because h_{sc} acts as an additive, product-specific offset that grows in high-snow regimes.

For applications focused on variability, the broadly coherent interannual signals across products support analyses based on anomalies and relative changes, provided baselines are handled consistently. For applications requiring absolute freeboard (and hence thickness), persistent sector-dependent offsets should be treated as an intrinsic source of uncertainty. Finally, we emphasise scope: this study is a compact comparison benchmark rather than an external validation, intended to clarify where products align and where retrieval choices introduce systematic differences.

5 Conclusions

We compare four gridded CryoSat-2 era (2013–2018) Antarctic winter (May–October) freeboard products (LEGOS, CCI, CSAO, Cryo-TEMPO) on a common 50 km EASE-2 grid, focusing on radar freeboard (h_{fr}) and derived sea-ice freeboard (h_{fi}). The main conclusions are:

1. **Shared large-scale structure, but persistent offsets.** All products reproduce the first-order winter freeboard pattern, with higher values in the Weddell and Ross sectors and lower values in the Indian and Amundsen-Bellingshausen sectors (Figure 1). However, sector-mean offsets relative to CCI persist through time at the centimetre scale (Figures 2–3).

2. **Snow-related conversion increases thickness-relevant spread from h_{fr} to h_{fi}.** Disagreement is typically larger for h_{fi} than for h_{fr}, consistent with product-to-product differences in the snow propagation-speed correction (h_{sc}). In the

https://doi.org/10.5194/egusphere-2026-662
Preprint. Discussion started: 12 February 2026

Western Weddell, the winter-mean h_{fi} spread across products reaches ∼0.12 m, compared with ∼0.05 m in the Ross sector (Figure 2; Table 1).

3. **High correlation does not imply agreement in absolute freeboard.** Interannual variability is broadly consistent across products ($r \sim 0.8$–0.95 in the Western Weddell and Ross sectors), yet systematic biases remain substantial, reaching ∼5–6 cm in the Western Weddell for both h_{fr} and h_{fi} relative to CCI (Figure 3).

Based on these conclusions, data users should consider how cross-product differences in baseline h_{fr} impact their analysis, and we suggest that future product development should prioritise tighter constraints on the snow propagation correction linking h_{fr} to h_{fi}.

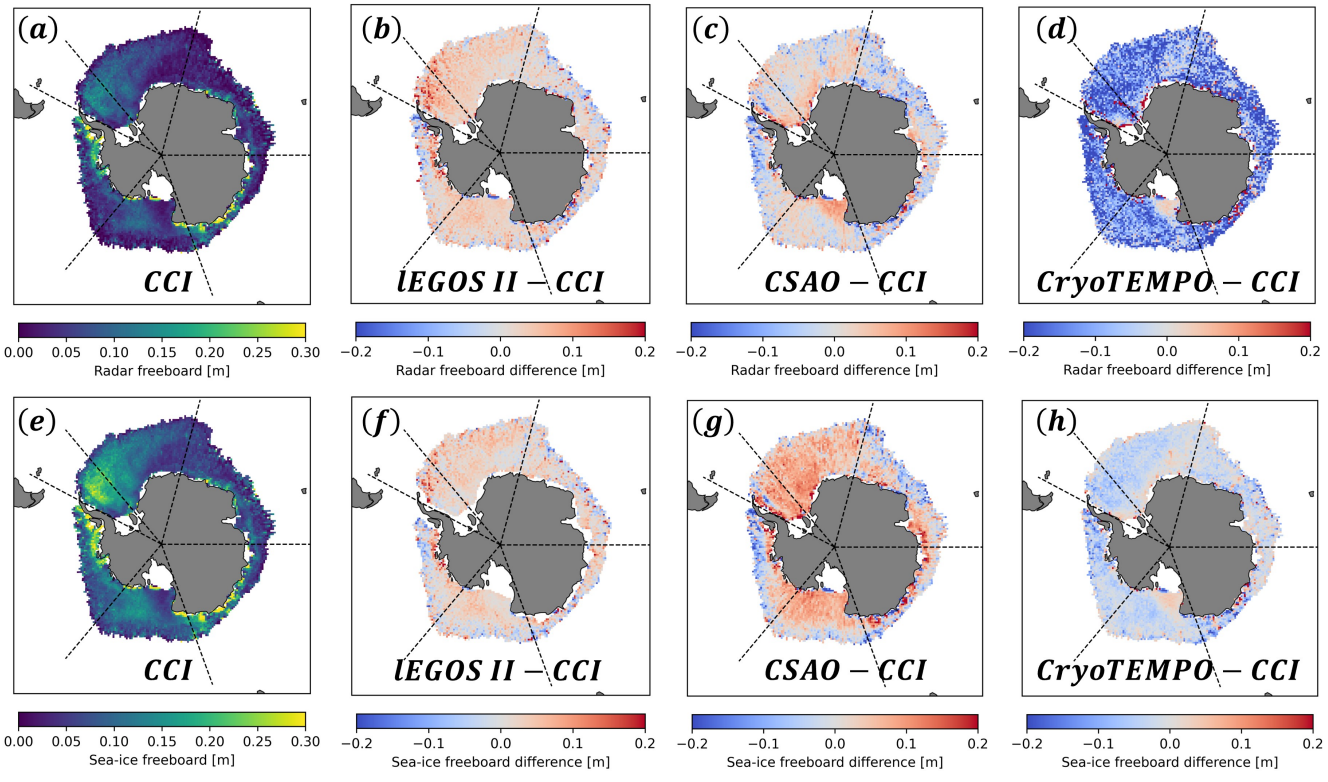

Figure 1. Winter-mean radar freeboard (a – d) and sea-ice freeboard (e – h) for the CryoSat-2 overlap period (2013–2018) on a 50 km EASE-2 grid. Panels (a, e) show the CCI winter mean; panels (b-d, f-h) show each product's mean difference relative to CCI (Δ = product − CCI). Difference maps use a diverging scale centred on zero and are evaluated on the shared spatial mask. Coherent regional offsets (not random noise) highlight retrieval-driven spread, especially in snow-influenced sectors.

https://doi.org/10.5194/egusphere-2026-662
Preprint. Discussion started: 12 February 2026

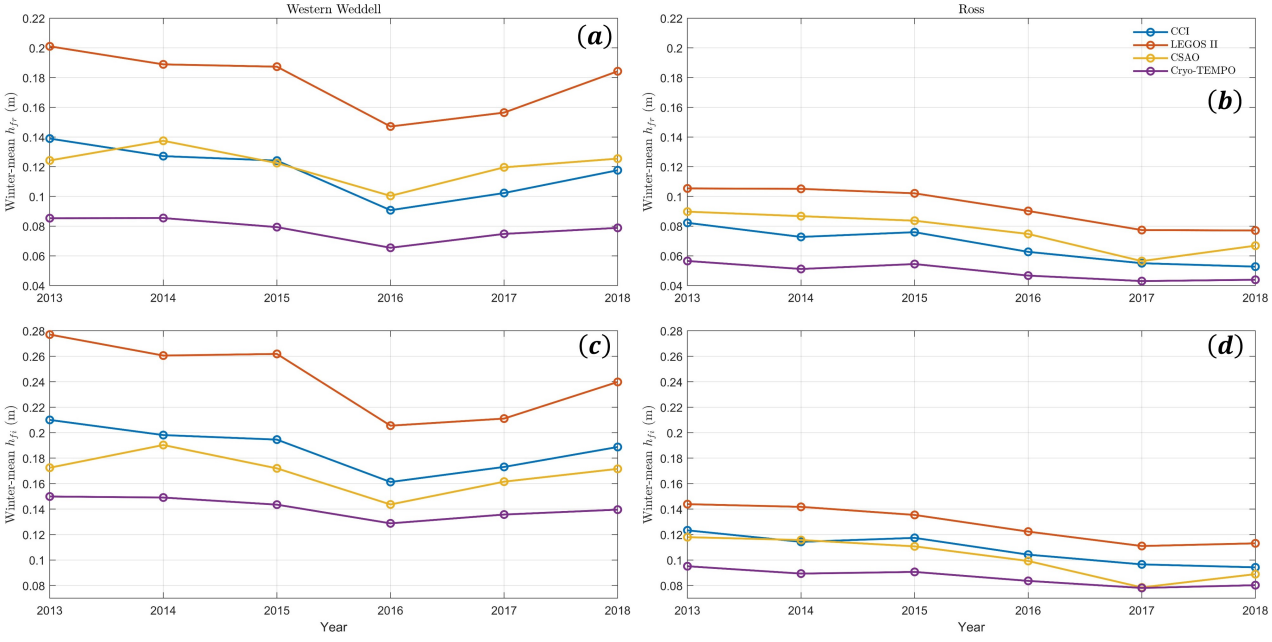

Figure 2. Interannual variability of winter-mean radar and sea-ice freeboard in the Western Weddell and Ross seas. Lines show sector means for each product computed on the shared grid and mask.

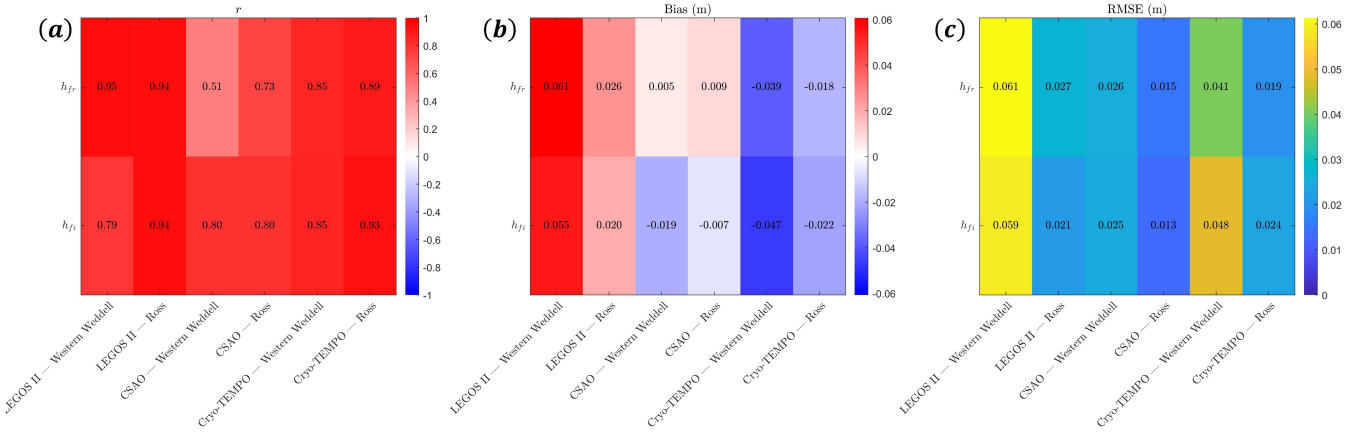

Figure 3. Summary agreement metrics relative to CCI for Western Weddell and Ross seas during CryoSat-2 winters. For each product and sector, we report (a) Pearson correlation (r), (b) mean difference (bias; product - CCI), and (c) RMSE for h_{fr} and h_{fi} using collocated grid cells on the shared mask.

https://doi.org/10.5194/egusphere-2026-662
Preprint. Discussion started: 12 February 2026

Table 1. CryoSat-2 era (2013–2018) multi-year austral-winter mean sector differences in (a) radar freeboard (Δh_{fr}) and (b) sea-ice freeboard Δh_{fi} relative to CCI (product minus CCI), computed on the common 50 km EASE-2 grid and common mask. Positive values indicate larger freeboards than CCI and negative values indicate smaller freeboards. Values are reported to 0.01 m; < 0.01 indicates an absolute difference smaller than 0.01 m.

	Western Weddell	Eastern Weddell	Indian	Pacific	Ross	Amundsen–Bellingshausen
Δh_{fr} (m)						
LEGOS II – CCI	0.06	0.03	0.01	< 0.01	0.02	0.02
CSAO – CCI	-0.04	-0.02	-0.03	-0.04	-0.01	-0.03
Cryo-TEMPO – CCI	-0.04	-0.02	-0.01	-0.04	-0.02	-0.03
Δh_{fi} (m)						
LEGOS II – CCI	0.05	0.03	0.02	0.01	0.02	0.02
CSAO – CCI	-0.07	-0.04	-0.04	-0.05	-0.03	-0.05
Cryo-TEMPO – CCI	-0.04	-0.02	-0.02	-0.03	-0.02	-0.03

Code and data availability. The code for analysis used in this study are publicly available on Zenodo via https://doi.org/10.5281/zenodo.18335479. All the satellite products used in this study are publicly available: **LEGOS**: https://www.LEGOS.altimetry.fr/en/data/products/ice-products/altimetry-sea-ice-products-from-ctoh.html. **CCI**: ftp://ftp.awi.de/sea_ice/projects/cci/crdp/v4p0/. **CSAO**: http://cryosat.mssl.ucl.ac.uk/csao/public-docs.html. **Cryo-TEMPO**: ftp://science-pds.cryosat.esa.int/. All the datasets used for analysis are publicly available on Zenodo via https://doi.org/10.5281/zenodo.18335479.

Author contributions. XL, SC, RT and PH have performed the analysis, writing and revision together.

Competing interests. One of the co-authors, PH, is a member of the editorial board of The Cryosphere.

Acknowledgements. This work contributes to Project 6 of the Australian Antarctic Program Partnership (ASCI000002) funded under the Australian Government's Antarctic Science Collaboration Initiative program. XL acknowledges support from the Institute for Marine and Antarctic Studies and the Australian Antarctic Program Partnership for this work. PH (PH, SC, RT) acknowledges support from the Australian Antarctic Science Program (AAS4496, AAS4506 (AAS4625)). PH & RT are supported through grant funding from the International Space Science Institute (Switzerland; ISSI; Project 501). The ISSI Team #501 as well as A.D. Fraser and M. Nikurashin (IMAS, Univ. Tasmania) are thanked for discussions on this topic.

https://doi.org/10.5194/egusphere-2026-662
Preprint. Discussion started: 12 February 2026

References

Andersen, O. B., McMillan, M., and Others: Cryo-TEMPO Product Handbook Version 4.1, https://earth.esa.int/eogateway/documents/20142/37627/CryoTEMPO-Thematic-Product-Handbook.pdf, 2025.

Comiso, J. C. and Nishio, F.: Trends in the sea ice cover using enhanced and compatible AMSR-E, SSM/I, and SMMR data, Journal of Geophysical Research: Oceans, 113, 2008.

Fons, S., Kurtz, N., and Bagnardi, M.: A decade-plus of Antarctic sea ice thickness and volume estimates from CryoSat-2 using a physical model and waveform fitting, The Cryosphere, 17, 2487–2508, 2023.

Fredensborg Hansen, R. M., Skourup, H., Rinne, E., Jutila, A., Lawrence, I. R., Shepherd, A., Høyland, K. V., Li, J., Rodriguez-Morales, F., Simonsen, S. B., et al.: Multi-frequency altimetry snow depth estimates over heterogeneous snow-covered Antarctic summer sea ice–Part 1: C/ S-, Ku-, and Ka-band airborne observations, The Cryosphere, 19, 4167–4192, 2025.

Garnier, F., Fleury, S., and Birol, F.: Sea Ice Freeboard, Snow Depth and Thickness Altimetric data products, https://www.aviso.altimetry.fr/fileadmin/documents/data/tools/hdbk_AltimetrySeaIce_CTOH.pdf, sALP-MU-P-EA-23415-CLS - Issue 2 rev 0 – 23/12/2019, 2019.

Garnier, F., Fleury, S., Garric, G., Bouffard, J., Tsamados, M., Laforge, A., Bocquet, M., Fredensborg Hansen, R. M., and Remy, F.: Advances in altimetric snow depth estimates using bi-frequency SARAL and CryoSat-2 Ka–Ku measurements, The Cryosphere, 15, 5483–5512, 2021.

Gaudelli, J., Rose, S., and Garnier, F.: CSAO: Deliverable DD-5 Experimental Dataset User Manual, http://cryosat.mssl.ucl.ac.uk/csao/DD5_V1.1.pdf, cSAO-TN-EDUM-5001; Version 1.1, 24 Nov 2022, 2022.

Huang, L. and Hajnsek, I.: A study of sea ice topography in the Weddell and Ross seas using dual-polarimetric TanDEM-X imagery, The Cryosphere, 18, 3117–3140, 2024.

Kacimi, S. and Kwok, R.: The Antarctic sea ice cover from ICESat-2 and CryoSat-2: freeboard, snow depth, and ice thickness, The Cryosphere, 14, 4453–4474, 2020.

Kurtz, N., Markus, T., Farrell, S., Worthen, D., and Boisvert, L.: Observations of recent Arctic sea ice volume loss and its impact on ocean-atmosphere energy exchange and ice production, Journal of Geophysical Research: Oceans, 116, 2011.

Kwok, R.: Simulated effects of a snow layer on retrieval of CryoSat-2 sea ice freeboard, Geophysical Research Letters, 41, 5014–5020, 2014.

Mallett, R. D., Lawrence, I. R., Stroeve, J. C., Landy, J. C., and Tsamados, M.: Brief communication: Conventional assumptions involving the speed of radar waves in snow introduce systematic underestimates to sea ice thickness and seasonal growth rate estimates, The Cryosphere, 14, 251–260, 2020.

Maykut, G. A.: Energy exchange over young sea ice in the central Arctic, Journal of Geophysical Research: Oceans, 83, 3646–3658, 1978.

Paul, S., Rinne, E., Hendricks, S., and Sallila, H.: CCI+ Sea Ice ECV - Sea Ice Thickness Algorithm Theoretical Basis Document (ATBD), https://doi.org/10.5281/zenodo.10605840, d2.1 Sea Ice Thickness Algorithm Theoretical Basis Document, 2024.

Rinne, E. and Hendricks, S.: CCI+ Sea Ice ECV - Sea Ice Thickness Product User Guide (PUG), https://doi.org/10.5281/zenodo.10605998, d4.2 Sea Ice Thickness Product User Guide, 2024.

Tilling, R., Ridout, A., and Shepherd, A.: Estimating Arctic sea ice thickness and volume using CryoSat-2 radar altimeter data, Advances in Space Research, 62, 1203–1225, 2018.

Willatt, R., Giles, K. A., Laxon, S. W., Stone-Drake, L., and Worby, A. P.: Field investigations of Ku-band radar penetration into snow cover on Antarctic sea ice, IEEE Transactions on Geoscience and remote sensing, 48, 365–372, 2009.

https://doi.org/10.5194/egusphere-2026-662
Preprint. Discussion started: 12 February 2026

Willatt, R., Mallett, R., Stroeve, J., Wilkinson, J., Nandan, V., and Newman, T.: Ku-and Ka-band polarimetric radar waveforms and snow depth estimation over multi-year Antarctic sea ice in the Weddell Sea, Geophysical Research Letters, 52, e2024GL112 870, 2025.